ACS APPLIED MATERIALS & INTERFACES

Research Article

www.acsami.org

Elucidating the Impact of Molecular Packing and Device Architecture on the Performance of Nanostructured Perylene Diimide Solar Cells

Eduardo Aluicio-Sarduy,[†] Ranbir Singh,[†] Zhipeng Kan,[†] Tengling Ye,[†,▽] Aliaksandr Baidak,[†,○] Alberto Calloni,[‡] Giulia Berti,[‡] Lamberto Duò,[‡] Agathaggelos Iosifidis,[⊥] Serge Beaupré,[§] Mario Leclerc,[§] Hans-Jürgen Butt,[∥] George Floudas,[⊥] and Panagiotis E. Keivanidis*[,#]

[†]Fondazione Istituto Italiano di Tecnologia, Centre for Nanoscience and Technology@PoliMi, Via Giovanni Pascoli 70/3, 20133 Milano, Italy

[‡]Dipartimento di Fisica, Politecnico di Milano, Piazza Leonardo da Vinci 32, I-20133, Milano, Italy

[§]Département de Chimie, Université Laval, Pavillon A-Vachon 1045, Avenue de la Médecine, Québec City, Québec, Canada G1 V 0A6

[∥]Max Planck Institute for Polymer Research, Ackermannweg 10, D-55128, Mainz, Germany

[⊥]University of Ioannina, Department of Physics, 451 10 Ioannina, Greece

[#]Cyprus University of Technology, Department of Mechanical Engineering and Materials Science and Engineering, Dorothea Bldg 511, 45 Kitiou Kyprianou Street, 3041 Limassol, Cyprus

Supporting Information

ABSTRACT: The performance of organic photovoltaic devices (OPV) with nanostructured polymer:perylene diimide (PDI) photoactive layers approaches the levels of the corresponding polymer:fullerene systems. Nevertheless, a coherent understanding of the difficulty for PDI-based OPV devices to deliver high power conversion efficiencies remains elusive. Here we perform a comparative study of a set of four different polymer:PDI OPV model systems. The different device performances observed are attributed to differences in the nanostructural motif of these composites, as determined by wide-angle X-ray scattering (WAXS) measurements. Long-range structural order in the PDI domain dictates (i) the stabilization energy and (ii) the concentration of the PDI excimers in the composites. The quenching of the PDI excimer photoluminescence (PL) is found to be insensitive to the former, but it depends on the latter. High PL quenching occurs for the low concentration of PDI excimers that are formed in PDI columns with a length comparable to the PDI excimer diffusion length. The stabilization of the PDI excimer state increases as the long-range order in the PDI domains improves. The structural order of the PDI domains primarily affects charge transport. Electron mobility reduces as the size of the PDI domain increases, suggesting that well-ordered PDI domains suffer from poor electronic connectivity. WAXS further reveals the presence of additional intermolecular PDI interactions, other than the direct face-to-face intermolecular coupling, that introduce a substantial energetic disorder in the polymer:PDI composites. Conventional device architectures with hole-collecting ITO/PEDOT:PSS bottom electrodes are compared with inverted device architectures bearing bottom electron-collecting electrodes of ITO/ZnO. In all cases the ZnO-functionalized devices surpass the performance of the conventional device analogues. X-ray photoelectron spectroscopy explains that in PEDOT:PSS-functionalized devices, the PDI component preferentially segregates closer to the hydrophilic PEDOT:PSS electrode, thus impeding the efficient charge extraction and limiting device photocurrent.

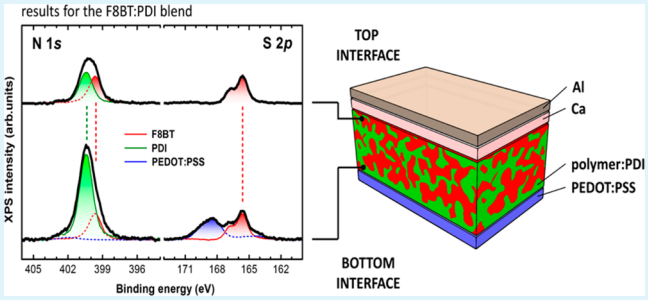

KEYWORDS: *organic photovoltaics, non-fullerene acceptors, perylene diimide, vertical phase separation, charge extraction*

1. INTRODUCTION

Today single-layer organic photovoltaic (OPV) devices can deliver power conversion efficiencies (PCE) on the level of 10%,[1] and large-area OPV fabrication can be achieved on mechanically robust and flexible substrates by utilizing low-cost deposition techniques that rely on high-throughput roll-to-roll production.[2] The basic components comprising the photoactive layer of an OPV device are an electron-accepting fullerene derivative mixed in an electron donor π-conjugated polymeric matrix.[3] Both fullerene and polymer components are soluble in most common organic solvents, and solution deposition of the polymer/fullerene mixture on planar substrates forms binary

Received: February 2, 2015
Accepted: March 30, 2015
Published: March 30, 2015

DOI: 10.1021/acsami.5b00827
ACS Appl. Mater. Interfaces 2015, 7, 8687−8698

composite films that comprise bicontinuous networks of the fullerene/polymer phases.[4,5]

After light absorption by the OPV photoactive layer components, a sequence of photophysical events results in the formation of electrons in the fullerene phase and holes in the polymer phase. In efficient OPV devices, these carriers are transported in the respective carrier-transporting phases and are extracted at the device electrodes. Despite the high PCE values reached today, the successful commercialization of OPV devices is impeded by high manufacturing costs.[6] A large fraction of these costs is due to the photoactive materials used and, particularly, due to the fullerene derivatives.[7,8] Moreover, fullerene derivatives are highly energy intensive components that increase the overall cumulative energy demand (CED) of a fullerene-based organic solar cell device.[9,10] Additionally, fullerenes absorb poorly in the visible; their contribution to the photocurrent generation by light capture is negligible. The replacement of fullerene derivatives by other molecular electron acceptors is expected to reduce both the total cost of the produced watt-peak (W_p) and the CED/W_p ratio and to bring the field of OPV devices closer to real market applications.

One class of small molecules that could provide an alternative for n-type OPV materials is the class of perylene diimide (PDI) derivatives. The superior light-absorbing strength of PDIs in the visible was early recognized, and efforts were made to incorporate PDI light absorbers in fullerene-based OPVs.[11] Advantageously, PDIs can be synthesized in a scalable and economical way, they are extremely photostable, and they can exhibit high electron mobility values in the order of 0.1 $cm^2/(V{\cdot}s)$.[12] Particularly for the case of OPV applications, the electron mobility in the PDI phase of the OPV photoactive layer is found to improve by 3 orders of magnitude after thermal treatment.[13]

In an effort to replace fullerene derivatives by PDIs acceptors, an understanding is sought for the parameters that dictate the morphology of nanostructured polymer:PDI blend films. For the case of the polymer:fullerene systems, the effect of fullerene aggregation and crystallization is well-understood. However, this knowledge cannot be fully extended to the case of blends of polymers with non-fullerene acceptors. In contrast to fullerenes, PDIs have a tendency to aggregate via $\pi-\pi$ stacking in the solid state.[14] Although PDI aggregation favors electron transport,[13] it may impede the dissociation of PDI excited states and limit the generation of charge species. Within a PDI aggregate, excitonic coupling effects are very strong,[15] and following light absorption, PDI excitons convert rapidly[16] to intermolecular states that exhibit an excimer-like luminescence[17] and an excimer-related characteristic transient absorption feature at 1600 nm.[18] On the basis of the lifetime of the PDI excimer luminescence and on the PDI excimer diffusion length,[19] the diffusion coefficient of the PDI excimer state is found to be very small, comparable to the diffusion coefficient of the archetypical pyrene excimer.[20] In efficient PDI-based OPVs, the slowly diffusive PDI excimers must first dissociate at the PDI/polymer interfaces. This can be achieved by fabricating photoactive layers where the PDI columnar stacks have an intracolumnar length that is comparable to the PDI excimer diffusion length.[21] Moreover, by introducing a small amount of disorder in the PDI phase, the electronic coupling of adjacent PDI aggregates is favored and the photogenerated electrons can be efficiently transported toward the device electrodes for their extraction to an external circuit.[22−24] The above suggest that the degree of order within the nanophases is an important parameter affecting device performance. The impact of molecular packing on the performance of PDI-based OPVs has been demonstrated with the use of solvent additives[25,26] that were found to improve the balance of the charge carrier mobility ratio and to suppress nongeminate recombination losses.[27] One of the questions that remains to be resolved is concerning the effect of the excimer stabilization energy ($E_{stab.}$) on the excimer dissociation efficiency. In particular, it is not yet clear if excimer dissociation can be more efficient in those polymer:-PDI blend films with the lower value of $E_{stab.}$, which corresponds to the difference between the energy of the PDI exciton in dilute solutions and the energy of the PDI excimer in the film.

In addition, the charge extraction efficiency, and consequently the PCE parameter of the PDI-based OPVs strongly depend on the type of charge-collecting electrode used in the device. For instance, it was suggested that the use of Al as the top electron-collecting (EC) electrode must be avoided due to the reactivity of Al with the PDI component, which results in the formation of an electron-blocking layer.[13] With respect to the conventional OPV device geometries, poly(styrenesulfonate)-doped polyethylene dioxythiophene (PEDOT:PSS) is typically used as the bottom hole-collecting (HC) electrode. The PEDOT:PSS electrode is used as the substrate onto which the polymer:PDI photoactive layer is deposited. In inverted OPV (i-OPV) device architectures, the bottom device electrode functions as the EC electrode and it is typically made of a solution-processable metal oxide such as ZnO.[28] For the polymer:PDI blend system of poly[4,8-bis-substituted-benzo[1,2-b:4,5-b′]dithiophene-2,6-diyl-*alt*-4-substituted-thieno[3,4-*b*]thiophene-2,6-diyl] (PBDTTT), it was found that the i-OPV device architecture delivers a PCE improved by 30% with respect to its conventional analogue.[21] More recently, it was shown that photoactive layers of a PBDTTT:BisPDI photoactive blend featuring a PDI bay-linked dimer can deliver a PCE as high as 4.3% in i-OPV devices bearing ZnO as the EC electrode.[29]

At this stage it is not entirely understood why inversion of the device polarity of PDI/polymer OPV systems significantly affects the performance of solar cell devices. More importantly, it is not yet clarified whether the positive effect of inverting the device geometry is system-specific or universal. Possible reasons are (i) a favorable vertical phase separation of the blend components, resulting in the segregation of the n-type (p-type) component closer to the EC (HC) electrode and/or (ii) optimized electronic coupling between the PDI component and the EC electrode, leading to a better charge extraction. Particularly, the latter was found to be critical in the performance of both conventional[21] and inverted[29] device geometries of PDI-based OPV blends that were engineered with electron-extracting interlayers. Recent reports demonstrated that the deposition of a fullerene self-assembled monolayer on the ZnO EC interlayer OPV devices of a PDI-dimer derivative can boost the device PCE to the level of 5.9%.[30] It was shown that PDI is more hydrophilic than the polymer matrices used as electron donors in OPV photoactive layers.[31] Since in conventional OPV devices the hydrophilic PEDOT:PSS is used as the HC electrode, it is very likely that PDI may segregate closer to PEDOT:PSS due the compatibility of the two materials. In that scenario, the segregation of the electron-transporting component close to the hole-extracting electrode would be unfavorable for efficient charge extraction,

DOI: 10.1021/acsami.5b00827
ACS Appl. Mater. Interfaces 2015, 7, 8687−8698

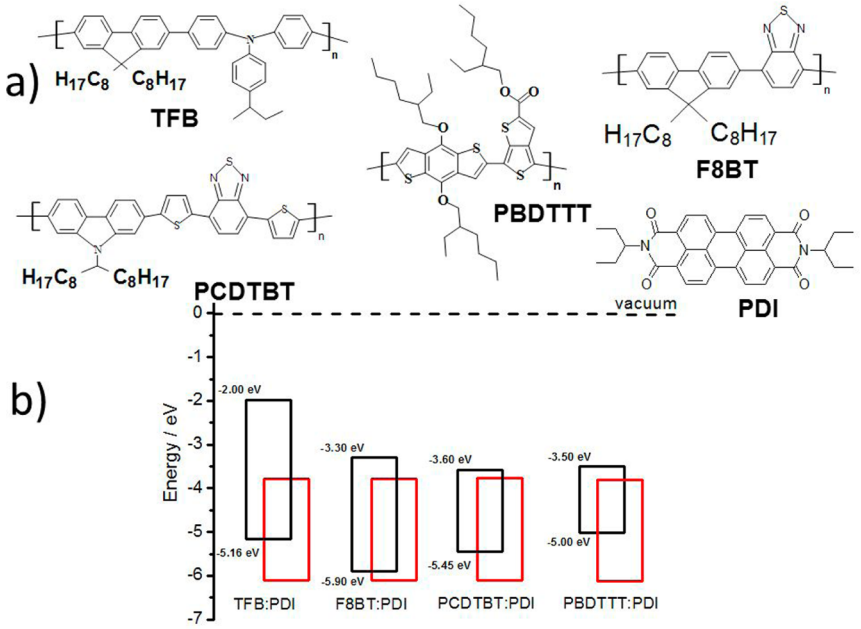

Figure 1. (a) The chemical structures of the materials used in this study. (b) The energetic offsets of the polymer/PDI heterojunctions for the systems of TFB:PDI,[17] F8BT:PDI,[17] PCDTBT:PDI,[33] and PBDTTT:PDI.[21]

and it would limit the photocurrent generation efficiency of the PDI-based OPV devices.

In this work we aim (i) to identify whether the excimer stabilization energy ($E_{stab.}$) plays a key role in the process of excimer dissociation in PDI-based OPV devices and (ii) to explain why i-OPV devices of PDI-based polymeric blends perform better than conventional ones. This is expected to open new pathways toward fabrication of efficient, fullerene-free OPV devices. For our study we use a monomeric PDI derivative that hitherto has given the highest device performance of monomer PDI-based OPV devices, with a PCE of 3.7%.[27] Instead of focusing our attention on the achievement of a high PCE value, we use a set of independent experimental techniques to study four model polymer:PDI OPV blends for identifying the combinatory effect of photophysical properties, structural motifs, and electrical response on the overall device efficiency. PDI dimers have led to PCE values of 6.3%;[32] however, elucidating the impact of structural order and device architecture on the performance of monomeric PDI OPV devices is expected to lead to equal PCE device performance, albeit with the use of less complex PDI structures of lower cost and lower cumulative energy demand.

Our study comprises two parts. In the first part, we discuss the impact of $E_{stab.}$ and structural perfection within the nanophases on the photocurrent generation and charge transport properties in PDI-based OPV devices. In the second part, in order to resolve the effect of inverting device polarity on the device performance, we study two different device geometries for each polymer:PDI system. In particular, we verify our hypothesis on the occurrence of a PDI concentration gradient at the bottom and the top regions of photoactive layers in conventional devices that utilize PEDOT:PSS as the HC electrode.

A comparison is performed between the electrical properties of as-spun devices with the conventional architecture of glass/ITO/PEDOT:PSS/polymer:PDI/Ca/Al (device type I) and of devices with the inverted architecture of glass/ITO/ZnO/polymer:PDI/V_2O_5/Ag (device type II). In all cases the PDI derivative *N*,*N*′-bis(1-ethylpropyl)perylene-3,4,9,10-tetracarboxylic diimide is used for preparing blend films with the polymers poly[9,9-dioctylfluorene-*co*-*N*-[4-(3-methylpropyl)]-diphenylamine] (TFB), poly(9,9′-dioctylfluorene-*co*-benzothiadiazole) (F8BT), poly[N-9′-heptadecanyl-2,7-carbazole-*alt*-5,5-(4′,7′-di-2-thienyl-2′,1′,3′-benzothiadiazole)] (PCDTBT), and PBDTTT.

2. EXPERIMENTAL DETAILS

The TFB and F8BT polymers were purchased from American Dye Source, whereas the PBDTTT polymer and the PDI derivative were purchased from Solarmer Materials Inc. The PCDTBT polymer was synthesized according to the synthetic protocol described before.[33] Reference films of polystyrene (PS):PDI composites were fabricated by using commercial PS purchased from Sigma-Aldrich. All materials were used as received without further purification for the fabrication of the polymer:PDI films and of the corresponding OPV devices. Thin films of polymeric and composite polymer:PDI layers with 60 wt % PDI content[17] were prepared by solutions in chloroform deposited on quartz substrates by spin-coating. Care was taken so that in all cases the resulting blend films had a typical thickness of 100 nm. UV−vis and PL spectra of these films were recorded according to the procedure previously described.[17] The preparation of conventional and inverted OPV devices and their electrical characterization were performed according to the protocols reported elsewhere.[21] Wide-angle X-ray scattering (WAXS) measurements were carried out with a Rigaku RA-Micro 7 desktop rotating-anode X-ray generator with a maximum power of 800 W and brightness of 18 kW/mm^2 [operated at a tube voltage of 40 kV and tube current of I = 12 mA (480 W)] utilizing a Cu target. The detection system was a MAR345 image plate area detector, and the sample-to-detector distance was set at 22.2 cm. Measurements from extruded fibers (extrusion temperature ∼150 °C) were done at 30 °C following fast cooling of the fibers to ambient temperature. From the recorded 2-D diffraction patterns the intensity distributions were obtained and are presented as a function of the scattering vector q [$q = (4\pi/\lambda)\sin(2\theta/2)$, where 2θ is the scattering angle]. Domain sizes were determined from the peak full width at half-maximum (fwhm). X-ray photoelectron spectroscopy (XPS) measurements were performed at room temperature in an ultrahigh vacuum (UHV) system (the base pressure was in the 10^{-8} Pa range) described in detail elsewhere.[34] The system was equipped with a Phoibos 150

DOI: 10.1021/acsami.5b00827
ACS Appl. Mater. Interfaces 2015, 7, 8687−8698

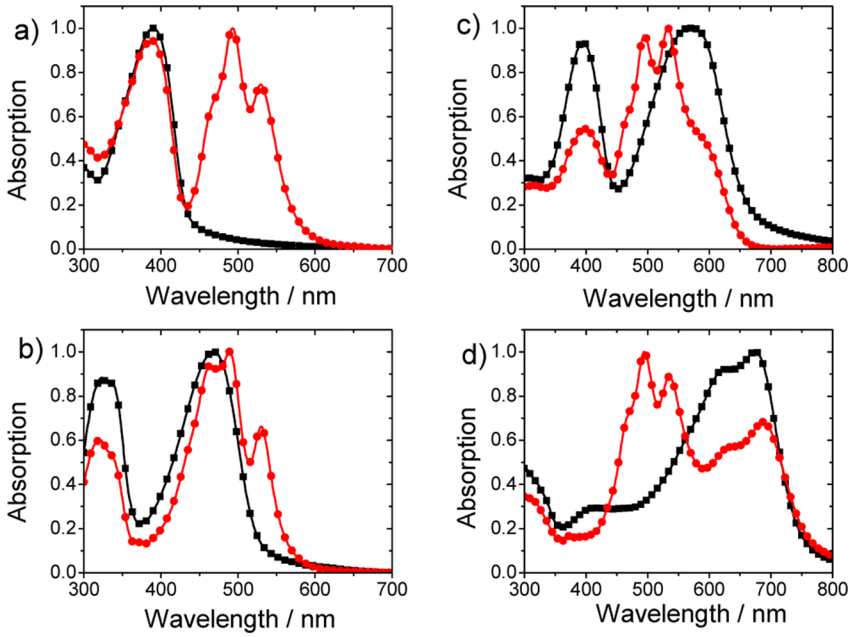

Figure 2. Normalized UV−vis spectra of thin films of the bulk polymers (black squares) and their blends with PDI (red circles) for (a) TFB and TFB:PDI, (b) F8BT and F8BT:PDI, (c) PCDTBT and PCDTBT:PDI, and (d) PBDTTT and PBDTTT:PDI. All films were deposited on quartz substrates.

hemispherical analyzer from SPECS GmbH, operated at a pass energy of 20 eV. Photoelectrons were excited by unmonochromatized Mg Kα radiation ($h\nu$ = 1253.6 eV), yielding an overall resolution (photons plus electrons) of 0.9 eV fwhm. The buried interfaces could be accessed by mechanically delaminating the polymer:PDI films by means of an UHV-compatible adhesive tape. Before delamination, the PEDOT:PSS substrates were first weakened by rinsing the samples with water, according to the method of ref 35, while ethanol was used to decrease the adhesion between the films and the ZnO surface, following ref 36. After being lifted off the substrate, the adhesive-supported films were transferred with the bottom interface upward on flat, p-doped Si substrates. This methodology is an alternative to ion sputtering, the latter usually employed to investigate the film composition at buried interfaces but often characterized by substantial alterations of the film properties that might adversely affect the accuracy of the XPS analysis.[35,37] Contact angle measurements were performed on the surfaces of the studied films deposited onto glass/ITO/PEDOT:PSS and glass/ITO/ZnO substrates, by using a drop shape analysis system (Dataphysics Instrument OCA 15EC). The contact angle values of the PEDOT:PSS and the ZnO layers were also determined. At least three measurements were performed for each sample in order to obtain the average contact angle values and their corresponding standard deviation, as determined by the drop shape analysis for the studied layers. An Agilent 5500 atomic force microscope (AFM) operating in tapping mode under ambient conditions was used for simultaneously recording topography and phase images of semicomplete devices with photoactive layers of TFB:PDI, F8BT:PDI, PCDTBT:PDI, and PBDTTT:PDI, deposited onto glass/ITO/PEDOT:PSS and glass/ITO/ZnO electrodes. Space charge limited current (SCLC) measurements were performed in unipolar devices of TFB:PDI, F8BT:PDI, PCDTBT:PDI, and PBDTTT:PDI for determining the charge transport properties of these systems. Hole-only devices and electron-only devices with a device structure of ITO/PEDOT:PSS/polymer:PDI blend/Au and ITO/ZnO/polymer:PDI blend/Ca/Al were prepared, respectively. A build-in voltage value of V_{bi} = 1.5 V was considered for the case of the electron-only devices.[21] In all samples prepared for WAXS, XPS, and SCLC, the PDI content was 60 wt %, except for the case of the PBDTTT:PDI system, where the optimum content of 70 wt % PDI[21] was used.

The chemical structures of the materials used in this study are shown in Figure 1a, and the energetic alignment of the frontier levels for each of the four polymer:PDI systems is shown in Figure 1b.

3. RESULTS

UV−Vis Absorption Spectroscopy. Figure 2 compares the UV−vis spectra of each of the bulk polymer donors as a single component film with the UV−vis spectra of the corresponding polymer:PDI blend film. It can be seen that at low photon energies the oscillator strength of the polymer donors and of the corresponding polymer:PDI binary mixtures gradually increases, following the series TFB, F8BT, PCDTBT, and PBDTTT. The absorption maxima of polymer donors shift gradually to longer wavelengths as $\lambda_{max\text{-}TFB}$ = 390 nm, $\lambda_{max\text{-}F8BT}$ = 467 nm, $\lambda_{max\text{-}PCDTBT}$ = 572 nm, and $\lambda_{max\text{-}PBDTTT}$ = 680 nm.

Solar Cell Characterization. OPV devices of the four systems were prepared on the basis of the type I and type II device geometries. Figure 3 presents the external quantum efficiency (EQE) and the J−V characteristics for these devices, whereas Table 1 reports the main device parameters, namely, the fill factor (FF), the open-circuit voltage (V_{oc}), the short-circuit current (J_{sc}), and the PCE of each device system.

On the basis of the absorption spectra of Figure 2 and the EQE data shown in Figure 3, it is found that for all systems the PDI component contributes significantly to the generation of device photocurrent by light absorption in the spectral region of 450−505 nm (see also the Supporting Information).

Two main observations can be made from these data. The first is that for a given type of device, the photocurrent generation efficiency and the device performance are increasing, following the series TFB:PDI, F8BT:PDI, PCDTBT:PDI, and PBDTTT:PDI. The second is that for all polymer:PDI photoactive layers, the performance of device type II surpasses that of device type I (see Table 1) when the photoactive layer thickness is kept unchanged for both device geometries.

Time-Integrated Photoluminescence Spectroscopy and Wide-Angle X-ray Scattering. We have performed

DOI: 10.1021/acsami.5b00827
ACS Appl. Mater. Interfaces 2015, 7, 8687−8698

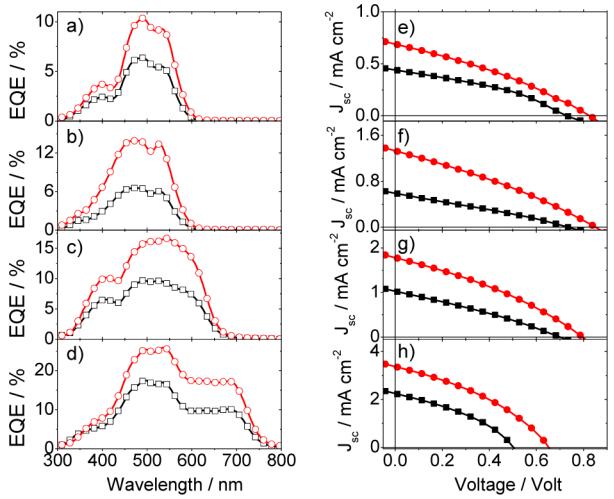

Figure 3. External quantum efficiency spectra of type I (open squares) and type II (open circles) devices of (a) TFB:PDI, (b) F8BT:PDI, (c) PCDTBT:PDI, and (d) PBDTTT:PDI. *J*–*V* characteristics of type I (filled squares) and type II (filled circles) devices of (e) TFB:PDI, (f) F8BT:PDI, (g) PCDTBT:PDI, and (h) PBDTTT:PDI.

photoluminescence (PL) quenching experiments on the polymer:PDI blend films. The increase in the PL quenching efficiency (Φ_q) of the PDI luminescence follows the same trend observed in the photocurrent generation efficiency of the corresponding OPV devices (see Tables 1 and 2).

After photoexcitation at 530 nm and with respect to a reference poly(styrene):PDI film, the PDI excimer PL intensity of the PCDTBT:PDI and PBDTTT:PDI blend films was reduced by nearly 100%, indicating an efficient dissociation of the PDI excimer state at the PDI/polymer interfaces in these systems (see the Supporting Information). For the TFB:PDI and F8BT:PDI blend films, a partial quenching of the PDI luminescence was found, suggesting that a high proportion of the PDI excimers is unable to undergo dissociation. The different degree of Φ_q in the studied systems could be discussed on the basis of three processes that cannot be disentangled by the time-integrated PL spectra alone. Inefficient quenching of the PDI excimer emission in the TFB:PDI and F8BT:PDI systems can be due to (i) the limited PDI excimer diffusion toward the PDI/polymer interfaces, (ii) the variation in the concentration of the PDI excimers in these blends, and (iii) a high excimer stabilization energy ($E_{stab.}$) that can impede PDI excimer dissociation.

Excimer diffusion can be discussed with respect to the intracolumnar PDI length, since the ability of the PDI excimer state to diffuse toward the PDI/polymer interfaces is limited by the extent at which the electronically coupled PDI monomers maintain their $\pi-\pi$ stacking coherence over a long spatial range. The concentration of the PDI excimer can be discussed on the basis of the fraction of the PDI molecules that have been converted to emissive intermolecular states in these blends. Finally, exciton stabilization can be discussed in terms of the electronic coupling strength between adjacent PDI monomers. In order to unravel these three possible origins of inefficient PL quenching, we first study the structural properties of the polymer:PDI blends and we then determine the PDI excimer concentration (C) and excimer stabilization energy ($E_{stab.}$) terms in each of these systems.

The structural motif of the TFB:PDI, F8BT:PDI, PCDTBT:PDI, and PBDTTT:PDI binary mixtures was studied by means of wide-angle X-ray scattering (WAXS) measurements on fibers extruded at elevated temperature (~150 °C) following fast cooling to ambient temperature. Given the thickness of the studied films in the photophysical studies (typically 100 nm), a similar structure as with the extruded fibers is expected. Both samples of spin-coated films and extruded fibers are made by virtue of irreversible thermodynamics, i.e., by applying a concentration gradient and shear force, respectively. Either process results in macroscopic orientation the degree of which is very sensitive to the actual experimental conditions. However, characteristic molecular and supramolecular distances obtained by the two deposition methods are identical.[38,39] Practically, the study of fibers by WAXS enables the straightforward extraction of the characteristic distances under investigation. Figure 4 presents the WAXS intensity profiles obtained by integration of the 2-D diffraction patterns. Structural features of long-range order are identified in all systems studied, albeit with different magnitude and strength. The (100) reflection associated with the stacking of polymer backbones is shown while the remaining peaks are associated with the crystalline PDI component. The assignment is based on separate diffraction measurements of the homopolymers, the PDI, and their blends at ambient conditions (see the Supporting Information) and as a function of temperature. The typical size of PDI domains (Ξ_{PDI}) in each of the composites is reported in Table 2 and it is found to follow the trend of $\Xi_{PBDTTT:PDI} < \Xi_{TFB:PDI} < \Xi_{F8BT:PDI} \approx \Xi_{PCDTBT:PDI}$. Likewise, the determined backbone-to-backbone correlations for the polymer nanodomains ($L_{polymer}$) are

Table 1. Main Device Metrics of the Polymer:PDI Organic Photovoltaic Devices Studied in This Work

device parameter	TFB:PDI	F8BT:PDI	PCDTBT:PDI	PBDTTT:PDI
		Conventional OPV Device Architecture		
V_{oc} (V)	0.73 ± 0.02	0.74 ± 0.01	0.70 ± 0.01	0.51 ± 0.01
FF (%)	26.4 ± 0.9	27.8 ± 0.8	29.5 ± 0.1	35.4 ± 0.2
J_{sc} (mA cm^{-2})	0.44 ± 0.02	0.58 ± 0.02	1.03 ± 0.02	2.3 ± 0.01
PCE (%)	0.14 ± 0.01	0.15 ± 0.01	0.25 ± 0.01	0.50 ± 0.01
PCE_{max} (%)	0.15	0.16	0.26	0.51
		Inverted OPV Device Architecture		
V_{oc} (V)	0.83 ± 0.01	0.85 ± 0.04	0.75 ± 0.02	0.57 ± 0.02
FF (%)	31.9 ± 1.6	30.4 ± 0.1	32.7 ± 0.4	36.7 ± 0.2
J_{sc} (mA cm^{-2})	0.68 ± 0.02	1.33 ± 0.31	1.80 ± 0.11	3.35 ± 0.08
PCE (%)	0.21 ± 0.01	0.41 ± 0.02	0.56 ± 0.01	1.00 ± 0.08
PCE_{max} (%)	0.22	0.43	0.57	1.10

DOI: 10.1021/acsami.5b00827
ACS Appl. Mater. Interfaces 2015, 7, 8687–8698

Table 2. Main Parameters of the Structural, Spectroscopic, and Electrical Characterization of the Polymer:PDI Blends and Corresponding Organic Solar Cells Studied in This Work

system	intracolumnar ξ_{PDI} (nm)	intercolumnar Ξ_{PDI} (nm)	domain $L_{polymer}$ (nm)	PL quenching	$E_{stab.}$ (meV)	μ_h [cm^2/(V·s)]	μ_e [cm^2/(V·s)]
TFB:PDI	12 ± 1	27 ± 1	1.1 ± 0.3	partial	334	(4.1 ± 0.1) × 10^{-8}	(4.5 ± 0.1) × 10^{-8}
F8BT:PDI	25 ± 1	43 ± 1	11 ± 0.5	partial	495	(0.4 ± 0.1) × 10^{-8}	(0.2 ± 0.1) × 10^{-8}
PCDTBT:PDI	14 ± 1	39 ± 1	2.7 ± 1	full	410	(5.2 ± 0.2) × 10^{-8}	(3.5 ± 0.2) × 10^{-8}
PBDTTT:PDI	12 ± 1	22 ± 1	4.3 ± 1	full	308	(9.4 ± 0.9) × 10^{-8}	(4.8 ± 0.2) × 10^{-8}

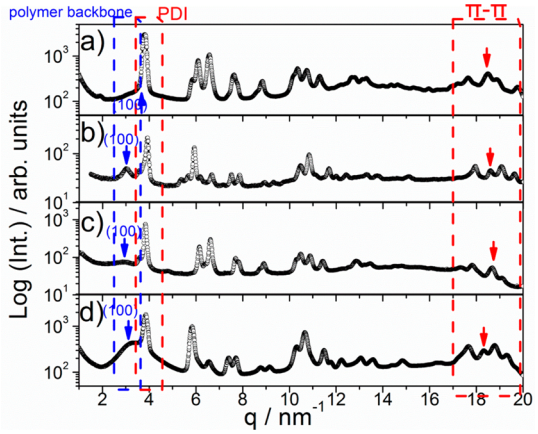

Figure 4. WAXS intensity distributions obtained from 2-D diffraction patterns plotted as a function of the scattering vector q: (a) TFB:PDI, (b) F8BT:PDI, (c) PCDTBT:PDI, and (d) PBDTTT:PDI. All measurements are made at 25 °C. The (100) reflection arising from polymer backbone−backbone correlations and the region arising from PDI π−π interactions are indicated by blue and red arrows, respectively.

reported in Table 2 and follow the trend of $L_{TFB:PDI} \leq L_{PCDTBT:PDI} \leq L_{PBDTTT:PDI} < L_{F8BT:PDI}$.

Finally, for each system, Table 2 reports the PDI intracolumnar correlation length (ξ_{PDI}) that is found to follow the trend of $\xi_{TFB:PDI} \approx \xi_{PBDTTT:PDI} \leq \xi_{PCDTBT:PDI} < \xi_{F8BT:PDI}$. Among all four systems investigated, the polymer domains and the PDI columns are better organized in the F8BT:PDI binary blend.

In the light of the structural information provided by WAXS, the incomplete quenching of the PDI PL emission intensity in the TFB:PDI and F8BT:PDI systems can be better understood. The PDI excimer diffusion length of a similar PDI derivative is D_{PDI} = 10 ± 5 nm,[19] which is comparable to the PDI columnar length in the TFB:PDI and PBDTTT:PDI blends. Nevertheless, the quenching efficiency of PDI luminescence is different in the two systems; for the direct photoexcitation of PDI at 530 nm, the PL quenching is partial in TFB:PDI and almost complete in PBDTTT:PDI (see the Supporting Information). Hence, matching the PDI excimer diffusion length with the columnar length of the PDI aggregate is not a sufficient condition for dissociating efficiently the PDI excimer state at the PDI/polymer interface. The WAXS data quantify the extent of nanophase separation of PDI and polymer in these blends, monitoring the concentration of the PDI/polymer. In combination with the electrical characterization results of the OPV devices (summarized in Table 1), it is evident that the trend for nanophase separation alone cannot explain the observed device performance. In the mesoscopic length scale, it is difficult to distinguish the degree of mixing between the PDI and the polymer component for each system. Atomic force microscopy imaging performed on the as-spun TFB:PDI, F8BT:PDI, PCDTBT:PDI, and PBDTTT:PDI blend films deposited on glass/ITO/ZnO electrodes found no evidence for the different mixing of the PDI and polymer components, which could potentially explain the different performance of the corresponding i-OPV devices (see the Supporting Information). Unlike the case of similar films deposited onto glass/ITO/PEDOT:PSS layers,[17] corrugations with a period of about 300 nm were observed in the surface topography of the ZnO-based samples.[40]

The PL spectra of the polymer:PDI blends provide additional information concerning the concentration (C) of the PDI excimers in each of the polymer:PDI blend films. Figure 5

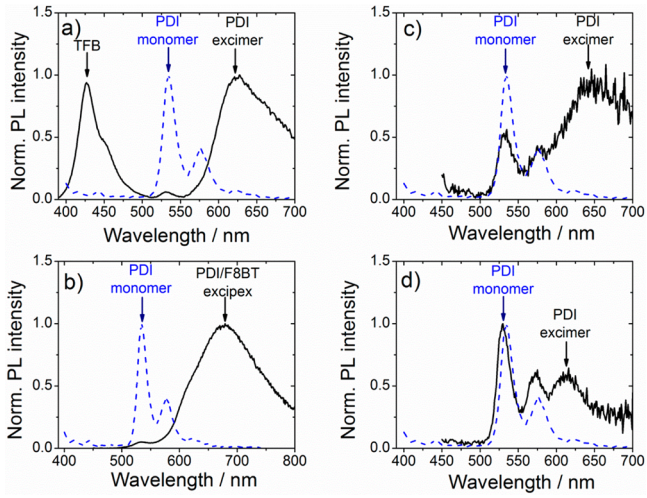

Figure 5. Time-integrated normalized photoluminescence (PL) spectra of as-spun films on quartz substrates (black lines) for photoactive films of (a) TFB:PDI, (b) F8BT:PDI, (c) PCDTBT:PDI, and (d) PBDTTT:PDI. The normalized PL spectrum of the PDI component in a dilute solution of toluene is also shown for reference purposes (dash lines). The spectra of F8BT:PDI, PCDTBT:PDI, and PBDTTT:PDI were recorded after photoexcitation of the films at 420 nm, and the spectra of TFB:PDI film and the PDI solution were recorded after photoexcitation at 390 nm. For all films the PDI content was 60 wt %.

presents the time-integrated PL spectra of these systems as obtained after excitation at 390 nm. The steady-state character of the PL data shown in Figure 5 cannot quantify the rate of PDI excimer formation in the polymer:PDI blends, but on the basis of the relative comparison of the PDI monomer PL band (535 nm) and the red-shifted PL band of the PDI intermolecular state, the concentration of the PDI intermolecular states in each film can be inferred. For each composite film, C corresponds to the PL intensity ratio of the PDI intermolecular species and the PDI monomer. We note that, according to WAXS findings (Table 2) the size of the nanostructured domains in these polymer:PDI blends is larger than 20 nm. Therefore, the probability for a resonance energy

DOI: 10.1021/acsami.5b00827
ACS Appl. Mater. Interfaces 2015, 7, 8687−8698

transfer between the emissive PDI excimer state and the low-energy gap polymers of PCDTBT and PBDTTT is very small unless energy transfer operates on the basis of a beyond-Forster mechanism.[21] Temperature-dependent PL quenching experiments in the PBDTTT:PDI system have further verified that in comparison to the charge-transfer-induced PL quenching of the PDI excimer luminescence, the energy-transfer-mediated PL quenching is a secondary process. This topic will be discussed separately elsewhere.

As Figure 5 shows, the PL signal of the TFB:PDI and F8BT:PDI blend films is completely different from the PDI PL spectrum in solution. The PL intensity at 535 nm is suppressed, indicating a vanishing concentration of the PDI monomeric form, and the PL spectra are red-shifted with respect to the solution PL spectrum; a featureless PL band dominates the PDI PL emission, which can be attributed to PDI intermolecular species.[17] The PL residue of the PCDTBT:PDI and PBDTTT:PDI blends exhibits similarities to the PDI spectrum in solution; however, the red-shifted spectral signature of the PDI excimer is also detected. In a previous composition-dependent study of the PDI luminescence in the photophysically inactive matrix of poly(styrene), the coexistence of PDI monomers and excimers was revealed as the PDI loading was increasing.[17] On the basis of the PL spectra of the polymer:PDI films shown in Figure 5, the concentration of the PDI intermolecular species, C, increases in the series $C_{PBDTTT:PDI} < C_{PCDTBT:PDI} < C_{TFB:PDI} \approx C_{F8BT:PDI}$.

Interestingly, the increase in the concentration of the PDI excimers follows the increase of the long-range order of the PDI domains (Ξ), as derived by WAXS (see Table 2). Therefore, the quenching efficiency of the PDI excimer is found to be inversely proportional to the concentration of the PDI intermolecular species that are formed in PDI columns with a length that is comparable to the PDI excimer diffusion length. This finding should be investigated separately by intensity-dependent photoluminescence and transient absorption characterization experiments of these polymer:PDI systems.

Next, we investigate whether a correlation can be established between the PL quenching efficiency (Φ_q) of the PDI luminescence in these systems and the value of the PDI excimer stabilization energy ($E_{stab.}$). In order to quantify spectroscopically the magnitude of $E_{stab.}$ in each polymer:PDI blend, the photon energy of the monomeric PDI PL emission of the films was compared with the photon energy of the PDI PL signal in a dilute solution of toluene. In Figure 5, the observed red-shift in the PDI PL signature of the PDI excimer of the polymer:PDI films with respect to the PL maximum of molecular PDI in solution offers a measure of the PDI stabilization energy after the formation of PDI intermolecular species. A similar picture is obtained when the films are photoexcited at lower photon energy, at 530 nm where the PDI component is directly photoexcited (see the Supporting Information). In the dilute solution, the PL emission of PDI is centered at 535 nm, as is expected for the monomeric PDI form. In contrast, in the solid state, the PL emission intensity of the PDI excimer in each of the four blends is centered at $PL_{TFB:PDI}$ = 625 nm, $PL_{F8BT:PDI}$ = 680 nm, $PL_{PCDTBT:PDI}$ = 650 nm, and $PL_{PBDTTT:PDI}$ = 615 nm. The corresponding $E_{stab.}$ values are $E_{stab.(TFB:PDI)}$ = 334 meV, $E_{stab.(F8BT:PDI)}$ = 495 meV, $E_{stab.(PCDTBT:PDI)}$ = 410 meV, and $E_{stab.(PBDTTT:PDI)}$ = 308 meV. We here note that for the F8BT:PDI system the relatively higher $E_{stab.}$ corresponds to an exciplex state formed between the F8BT and the PDI components. Previous delayed luminescence spectroscopic studies on the F8BT:PDI system verified that emissive PDI/F8BT exciplexes further stabilize and immobilize the excited states of PDI at the PDI/F8BT interface.[41] Table 2 presents the overview of the $E_{stab.}$ and Φ_q values of the studied systems, and no correlation between the $E_{stab.}$ and Φ_q terms was found.

To this end, our results have not yet explained what determines the strength of electronic coupling between the PDI monomers in the polymer:PDI blend films so that the PDI excimer stabilization can obtain different values. Composition-dependent PL studies of PDI blends in the photophysically inert matrix of polystyrene have also shown that the peak PL of the PDI excimer emission depends on the local environment of the PDI component.[17] For the emissive PDI excimers in columnar stacks, the extent of the red-shift in the excimer PL band depends on the lateral shifts and the rotation of the monomeric units against each other. The magnitude of the red-shift depends on the efficiency with which the intermolecular vibrations are coupled to the electronic transition. Interestingly, for the herein studied polymer:PDI blends, the progression in the amount of $E_{stab.}$ is not reflected in the trend of increasing ξ_{PDI} (local order in the PDI columns), but it follows the increase in Ξ_{PDI} (long-range order in the PDI domains). This is a rather unexpected result given that according to the WAXS data, the intermolecular distance of the $\pi-\pi$ stacking in the four polymer:PDI systems is the same. Therefore, it is conceivable that a longer range excitonic coupling may take place between PDI columnar aggregates present in a well-ordered PDI domain. In that case, PDI excimer formation initiates from the stacking of adjacent monomers, but it is better facilitated via the intermolecular coupling of adjacent PDI columnar aggregates. In intercolumnar interactions, the coupling strength will depend on the rotation of the interacting columns against each other.[42] Further theoretical studies are sought for elucidating in detail the effect of intercolumnar aggregate interactions on the excitonic coupling process of disk-shaped compounds similar to the PDI system in polymer blends.[43]

Deeper insight can be gained with the WAXS data concerning the electronic coupling of the PDI monomers within a PDI column. We have performed temperature-dependent WAXS measurements on all four polymer:PDI blend systems in a temperature range between room temperature and 200 °C. At high temperatures, where the organization of the PDI aggregate is maximized, we have identified the WAXS reflections that correspond to the PDI $\pi-\pi$ stacking. Figure 6 presents a magnification of the room temperature WAXS data shown in Figure 4, by focusing in the region of 17–20 nm^{-1}, where a distribution of $\pi-\pi$ stacking configurations can be seen. The dominant $\pi-\pi$ stacking reflection is indicated by an arrow for each system. The diffraction patterns are dominated by the crystal packing of PDI molecules, which is similar but not identical in the four blends.

Charge Transport Properties. We have performed charge transport measurements in unipolar devices (see the Supporting Information), and we have deduced the zero-field electron and hole mobility values of all four polymer:PDI OPV blend films in their as-spun state. Table 2 reports these carrier mobility values as determined on the basis of the Mott–Gurney equation, by taking into account the Poole–Frenkel effect.[21] Both electron and hole mobility values are found to be on the order of 10^{-8} $cm^2/(V \cdot s)$, which is not surprising given the fact that in as-spun PDI-based systems the organization of the electron- and hole-transporting phases is low. Like in the case

DOI: 10.1021/acsami.5b00827
ACS Appl. Mater. Interfaces 2015, 7, 8687–8698

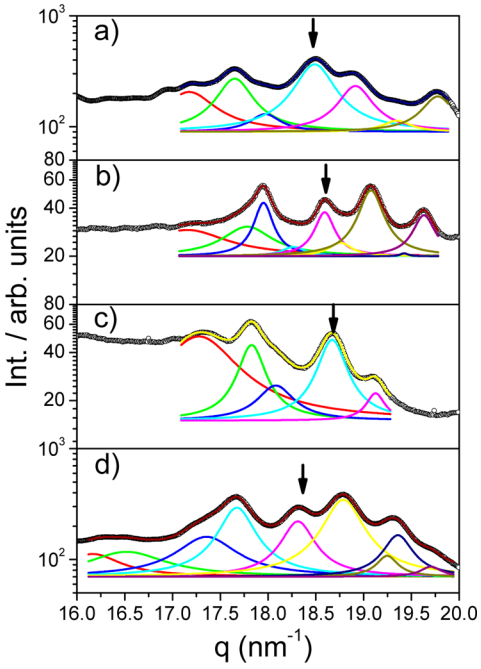

Figure 6. WAXS intensity distributions obtained from 2-D diffraction patterns plotted as a function of the scattering vector q in the region of 17−20 nm^{-1}, where the PDI $\pi-\pi$ interactions are indicated by black arrows: (a) TFB:PDI, (b) F8BT:PDI, (c) PCDTBT:PDI, and (d) PBDTTT:PDI. All measurements are made at 25 °C.

of similar PDI-containing OPV blend films,[13,21] after annealing the thermally induced formation of PDI aggregates is expected to result in the significant improvement of the electron mobility. Nonetheless, the study of the charge transport properties in the as-spun state of these systems, in relation to their structure as studied by WAXS, provides valuable insight concerning the structure−transport correlation in PDI-based OPV systems. This correlation is highlighted below in the Discussion section.

Contact Angle Measurements and X-ray Photoelectron Spectroscopy. We now focus on the differences between type I and type II devices. We carried out static (as placed) contact angle measurements on PEDOT:PSS and ZnO layers deposited on glass/ITO substrates in an identical fashion, as in the case of the device fabrication protocol (Figure 7). We

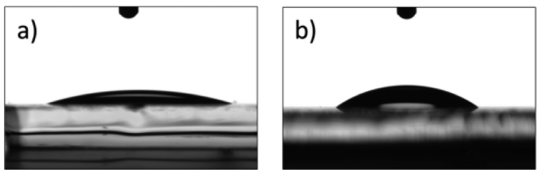

Figure 7. Water droplets on layers of (a) PEDOT:PSS and (b) ZnO deposited on glass/ITO substrates.

found that the PEDOT:PSS layer is more hydrophilic than the ZnO layer, exhibiting a contact angle of 15° ± 2°, much lower than the contact angle of 34° ± 2° for ZnO. According to these results, the hydrophilic PDI component should accumulate closer to the PEDOT:PSS/polymer:PDI interface than to the ZnO/polymer:PDI interface. In a previous report, we have shown that the use of a thin polymeric interlayer leads to the efficient dispersion of the PDI component in the bulk of PDI-based polymeric OPV blends by suppressing the PDI enrichment at the PEDOT:PSS/blend interface.[31] A similar effect is expected here to take place when a ZnO layer is used in the type II device architecture.

The XPS measurements were performed on a series of films of the four polymer:PDI blends, as-spun on PEDOT:PSS and ZnO substrates. The photoemission spectra were acquired at grazing electron emission, resulting in a probed depth of about 5 nm. We evaluated the PDI concentration from the measured XPS intensities at the air/film (top) interface and at the exposed (bottom) interface with the substrate according to the method illustrated in the Supporting Information. Figure 8 shows the retrieved PDI concentrations for the films spin-coated on (a) glass/ITO/PEDOT:PSS and (b) glass/ITO/ZnO substrates. We observed (Figure 8a) a clear tendency toward the segregation of PDI molecules close to the PEDOT:PSS substrate (bottom interface), in analogy with a previous XPS study focused on the PBDTTT:BisPDI system.[29] At variance with the PEDOT:PSS case, PDI segregation does not take place at the interface with the ZnO substrate, at least in three out of four blends considered for the present study (Figure 8b). In addition, we detected similar PDI concentrations at the top and bottom interfaces of the ZnO/F8BT:PDI and ZnO/PCDTBT:PDI films, suggesting the presence of a rather uniform distribution of the PDI molecules in the organic layer. Although several attempts were made, the determination of the PDI concentration at the bottom interface by film delamination proved to be impossible for the ZnO/PBDTTT:PDI samples. We also acquired a set of photoemission spectra at normal electron emission (see the Supporting Information), corresponding to a probed depth of about 10 nm and, consequently, to a smaller surface sensitivity. These normal emission data confirm, for all the substrate/film combinations, the PDI concentration behavior shown in Figure 8. In most cases, we detected a lowering of the PDI concentration at the top interface, going from normal to grazing emission. This is consistent with the formation of a thin layer (a few nanometers thick) of reduced PDI concentration, due to the segregation of the polymeric component toward the surface in order to minimize the free energy of the system.[35] At the bottom interface, an increased PDI concentration is observed at grazing emission for the polymer:PDI films spin-coated on PEDOT:PSS, suggesting the formation of a PDI-enriched layer within a region some nanometers from the PEDOT:PSS interface. The presence of a similar PDI concentration gradient is not evident at the interface of the polymer:PDI films with ZnO, due to smaller differences between the PDI concentrations detected at normal and grazing emission. It is worth considering in greater detail the results obtained for the TFB:PDI films. We detected a 100% PDI concentration at the bottom interface with PEDOT:PSS, irrespective of the XPS probing depth (Figure 8a), and an unexpected (if compared to the results obtained for the other blends) imbalance in the PDI concentration between the top and the bottom interfaces for the films spin-coated on ZnO (Figure 8b). These results again clearly demonstrate the influence of the substrate in the process of polymer/PDI segregation. More than that, they show that the presence of compositional gradients on a length scale larger than that of the interface layers probed in the present experiment cannot be generally excluded.

DOI: 10.1021/acsami.5b00827
ACS Appl. Mater. Interfaces 2015, 7, 8687−8698

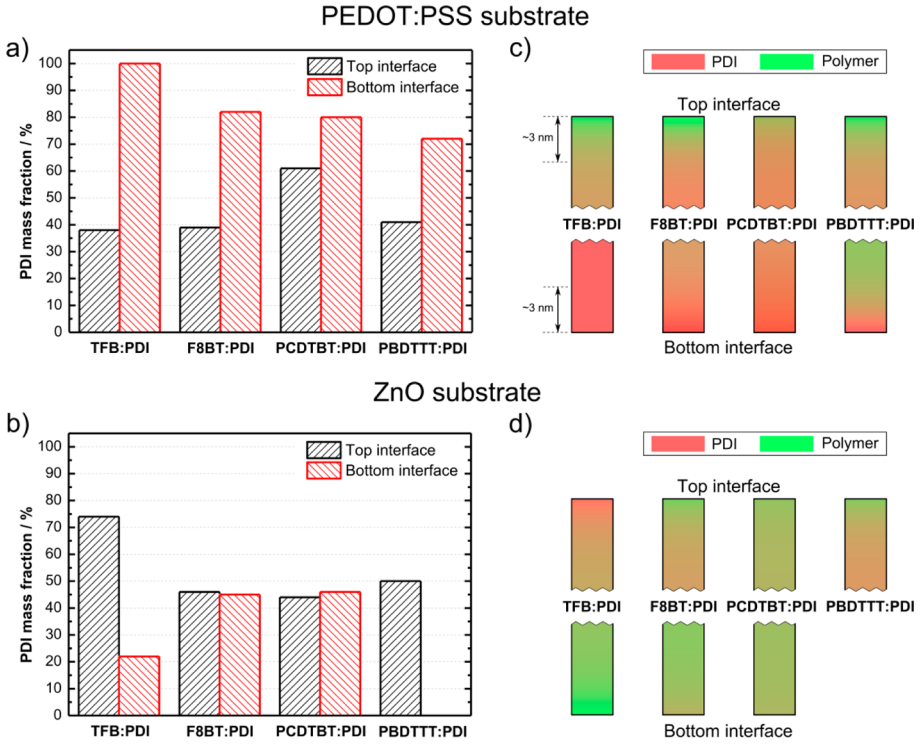

Figure 8. PDI concentration (10% quantification error) at the top (black-shaded columns) and bottom (red-shaded columns) interfaces of the as-spun polymer:PDI films deposited on (a) glass/ITO/PEDOT:PSS and (b) glass/ITO/ZnO electrodes. The PDI concentration at the bottom interface of the ZnO/PBDTTT:PDI film could not be determined. Schematic diagrams depicting the assumed vertical concentration gradient of the PDI component in each type of electrode; polymer:PDI blend is deposited on (c) glass/ITO/PEDOT:PSS and (d) glass/ITO/ZnO electrode. The color code for the schematics c and d is set by the experimentally obtained data, by assuming an exponential variation of the PDI concentration on a length scale comparable to the depth probed by XPS (see the text).

4. DISCUSSION

The trend in the increased light-absorbing power of the polymer:PDI blends at lower photon energies (longer wavelengths) and in the increased quenching efficiency of the PDI luminescence can explain the observed trend in the electrical performance of the polymer:PDI devices (both type I and type II). More light absorption results in the formation of a higher concentration of neutral excited states, which when efficiently dissociate at the PDI/polymer interfaces lead to photocurrent generation. Moreover, in the light of the XPS findings, the inferior performance of device type I is clearly attributed to the general tendency of the PDI component to accumulate closer to the hydrophilic surface of the PEDOT:PSS HC electrode. Nonetheless, the J_{sc} of the PBDTTT:PDI devices (both type I and II) is about 2 times higher than that of the PCDTBT:PDI devices, despite the comparable PL quenching efficiency observed in the two blends. The inferior performance of the PCDTBT:PDI system can be understood as the result of the differences found in the structural features of the PDI domain size that inevitably affect the processes of charge transport and charge recombination. Regardless of the high generation yield of free carriers after PDI excimer dissociation, an unfavorable microstructure will result in poor charge transport and in increased photocurrent losses caused by an enhanced charge recombination rate. According to the WAXS results, the PDI domain size is almost two times higher in the PCDTBT:PDI blend ($\Xi_{PCDTBT:PDI}$ = 39 ± 1 nm) than in the PBDTTT:PDI blend ($\Xi_{PBDTTT:PDI}$ = 22 ± 1 nm). Although this is found to result in an increased electronic coupling of PDI columns within a PDI domain, it does not seem to help the connectivity of adjacent PDI domains.[44] In fact, a reduction can be seen in the electron mobility of the as-spun polymer:PDI systems as the domain size of the PDI phase increases (see Table 2). This observation is in line with previous discussions on the effect of local disorder on the effective electronic coupling of electron-transporting domains and on the efficient macroscopic charge transport properties of organic semiconductors.[22,45,46] The results shown in Table 2 confirm that some amount of local disorder in the PDI crystallites is necessary for achieving efficient electronic coupling between adjacent PDI domains and for increasing the macroscopic electron transport in the pathways that are defined by the trajectories that connect the device electrodes. This is well-demonstrated by the F8BT:PDI blend possessing the highest structural order both for the PDI domains and polymer domains but having the smallest PCE. Likewise, the PBDTTT:PDI blend with the highest PCE possesses the lowest order within the PDI domains.

Photoexcitation-intensity-dependent measurements of J_{sc} and V_{oc} for all devices of both types suggest that nongeminate charge recombination events are important loss pathways in PDI-based OPVs. The onset of bimolecular recombination losses in PDI-based OPV blends was also suggested by recent transient absorption studies.[47] For all device systems of type I in this study, the device V_{oc} saturates when the photoexcitation intensity becomes larger than 0.08 Sun (see Supporting Information), indicating severe recombination losses at illumination intensities close to 1 Sun. The V_{oc} dependence is different in device type II, where the V_{oc} increases linearly with the logarithm of photoexcitation intensity (ln I_{exc}) up to 1 Sun illumination. At all cases, the slope of the V_{oc} dependence on ln

DOI: 10.1021/acsami.5b00827
ACS Appl. Mater. Interfaces 2015, 7, 8687−8698

I_{exc} reaches values that are 4−5 times higher than k_BT/q. This is in stark contrast to what has been observed in fullerene-based[48] or in PDI-dimer-based[30] OPV devices, and it implies a large degree of energetic disorder[49,50] in the photoactive layers of organic solar cells prepared by the PDI monomeric derivative. Increased energetic disorder should be expected given the distribution of the $\pi-\pi$ intermolecular packing motifs found in the WAXS data of Figures 4 and 6. Recent transient photovoltage and photocurrent measurements on OPV devices of the PBDTTT:PDI system also identified the occurrence of energetic disorder and inferred the presence of energetic traps.[27] The detailed analysis of the WAXS data is expected to quantify further the structural motifs of the PDI packing that result in the formation of charge trapping sites in the polymer:PDI composite systems. However, this discussion is beyond the scope of the present work and it will be presented separately elsewhere.

5. CONCLUSIONS

In conclusion, we have performed a combinatory study for elucidating the key physicochemical factors that control the performance of PDI-based OPV devices. For a series of four different PDI-based OPV material combinations, we have addressed the effect of structural order on the main parameters that influence the performance of the corresponding PDI-based OPV devices. Time-integrated PL spectroscopy and WAXS characterization measurements found that the stabilization energy $E_{stab.}$ of the PDI excimer state in these systems is not primarily affecting the dissociation efficiency of the PDI excimer. Instead, excimer dissociation and, consequently, PDI PL quenching is favored when the concentration of the PDI excimers is low and when the length of the PDI columnar aggregate is comparable to the excimer diffusion length. WAXS measurements resolved the extent to which the PDI excited state is stabilized by showing that $E_{stab.}$ is the result of an intercolumnar PDI excitonic coupling in the PDI domain. Hence, both the concentration of the PDI excimer and the corresponding $E_{stab.}$ term increase with the increase of the PDI domains. On the other hand, increased local order prevents the efficient interconnection of adjacent PDI domains, and large PDI domains suffer from poor connectivity and low electron mobility. As a result, nongeminate recombination events limit the device photocurrent in these systems. WAXS further revealed a distribution of PDI intermolecular interactions on top of the prominent direct $\pi-\pi$ stacking of the PDI monomers.

Finally, we have carefully addressed the dependence of the photocurrent generation efficiency on the type of electrode on which the polymer:PDI photoactive layer is deposited. It is confirmed that the PDI component has a strong affinity for the hydrophilic PEDOT:PSS hole-collecting electrode. Concurrently, the resulting vertical phase separation profile for polymer:PDI photoactive layers is impeding the efficient charge carrier extraction in the corresponding PEDOT:PSS-based devices. The detrimental effect of this unfavorable vertical phase separation can be rectified when inverted devices are fabricated in which the photoactive layer of polymer:PDI blend film is deposited on an electron-collecting ZnO layer. The ZnO interlayer is less hydrophilic than PEDOT:PSS and helps the homogeneous dispersion of the polymer and PDI components across the bulk of the polymer:PDI blend films. Alternatively, the use of a thin polymeric hole-transporting interlayer[24] may support the homogeneous distribution of the PDI component across the polymer:PDI OPV film.

Our results offer valuable guidelines for fabricating OPV devices of low cumulative energy demand by utilizing PDI-based photoactive layers. Mastering the accurate tuning of the layer microstructure in PDI OPV layers can pave the way for the realization of fullerene-free solar cell devices at larger scale by roll-to-roll-compatible processing techniques. The conclusions drawn from this study can be translated to a higher-performing PDI-based system fabricated with polymer donors exhibiting higher performances. At present, a deeper understanding of the effect of the structural motifs in PDI-based photoactive layers on solar cell device performance is provided. By ensuring that the PDI component of the photoactive layers is homogeneously distributed across the device electrodes and that the PDI domains are properly connected, also thanks to a certain degree of local disorder, the unfavorable effects of impeded charge extraction and enhanced charge recombination can be avoided. In that way, the percolation of photogenerated electrons across the PDI domains can be promoted and the overall device performance can be maximized.

■ ASSOCIATED CONTENT

Ⓢ Supporting Information

Normalized UV−vis and EQE spectra, time-integrated PL spectra, WAXS structural data, SCLC charge transport data, additional XPS information, atomic force microscopy images, and light-intensity-dependent open-circuit voltage characterization. This material is available free of charge via the Internet at http://pubs.acs.org.

■ AUTHOR INFORMATION

Corresponding Author

*E-mail: p.keivanidis@cut.ac.cy.

Present Addresses

[▽]School of Science, Harbin Institute of Technology, 92 West Dazhi St., Nan Gang District, Harbin 150001, P. R. China.

[○]Dalton Cumbrian Facility, Dalton Nuclear Institute, The University of Manchester, Westlakes Science & Technology Park, Moor Row, Cumbria, CA24 3HA, UK.

Author Contributions

E.A.-S and R.S. contributed equally.

Notes

The authors declare no competing financial interest.

■ ACKNOWLEDGMENTS

A.C. is funded by Fondazione Cariplo (2012-09-04 SECARS project).

■ REFERENCES

(1) Green, M. A.; Emery, K.; Hishikawa, Y.; Warta, W.; Dunlop, E. D. Solar Cell Efficiency Tables (version 43). *Prog. Photovoltaics* **2014**, *22*, 1−9.

(2) dos Reis Benatto, G. A.; Roth, B.; Madsen, M. V.; Hösel, M.; Søndergaard, R. R.; Jørgensen, M.; Krebs, F. C. Carbon: The Ultimate Electrode Choice for Widely Distributed Polymer Solar Cells. *Adv. Energy Mater.* **2014**, *4*, 1400732.

(3) Service, R. F. Outlook Brightens for Plastic Solar Cells. *Science* **2011**, *332*, 293−293.

(4) Sariciftci, N. S.; Smilowitz, L.; Heeger, A. J.; Wudl, F. Photoinduced Electron-Transfer from a Conducting Polymer to Buckminsterfullerene. *Science* **1992**, *258*, 1474−1476.

DOI: 10.1021/acsami.5b00827
ACS Appl. Mater. Interfaces 2015, 7, 8687−8698

(5) Halls, J. J. M.; Walsh, C. A.; Greenham, N. C.; Marseglia, E. A.; Friend, R. H.; Moratti, S. C.; Holmes, A. B. Efficient Photodiodes from Interpenetrating Polymer Networks. *Nature* **1995**, *376*, 498−500.
(6) Azzopardi, B.; Emmott, C. J. M.; Urbina, A.; Krebs, F. C.; Mutale, J.; Nelson, J. Economic Assessment of Solar Electricity Production from Organic-Based Photovoltaic Modules in a Domestic Environment. *Energy Environ. Sci.* **2011**, *4*, 3741−3753.
(7) Mulligan, C. J.; Wilson, M.; Bryant, G.; Vaughan, B.; Zhou, X.; Belcher, W. J.; Dastoor, P. C. A Projection of Commercial-Scale Organic Photovoltaic Module Costs. *Sol. Energy Mater. Sol. Cells* **2014**, *120* (Part A), 9−17.
(8) Machui, F.; Hösel, M.; Li, N.; Spyropoulos, G. D.; Ameri, T.; Søndergaard, R. R.; Jørgensen, M.; Scheel, A.; Gaiser, D.; Kreul, K.; Lenssen, D.; Legros, M.; Lemaitre, N. e.; Vilkman, M.; Välimäki, M.; Nordman, S.; Brabec, C. J.; Krebs, F. C. Cost Analysis of Roll-to-Roll Fabricated ITO Free Single and Tandem Organic Solar Modules Based on Data from Manufacture. *Energy Environ. Sci.* **2014**, *7*, 2792−2802.
(9) Anctil, A.; Babbitt, C. W.; Raffaelle, R. P.; Landi, B. J. Material and Energy Intensity of Fullerene Production. *Environ. Sci. Technol.* **2011**, *45*, 2353−2359.
(10) Anctil, A.; Babbitt, C. W.; Raffaelle, R. P.; Landi, B. J. Cumulative Energy Demand for Small Molecule and Polymer Photovoltaics. *Prog. Photovoltaics* **2013**, *21*, 1541−1554.
(11) Baffreau, J.; Leroy-Lhez, S.; Hudhomme, P.; Groeneveld, M. M.; van Stokkum, I. H. M.; Williams, R. M. Superabsorbing Fullerenes: Spectral and Kinetic Characterization of Photoinduced Interactions in Perylenediimide−Fullerene-C_{60} Dyads. *J. Phys. Chem. A* **2006**, *110*, 13123−13125.
(12) Struijk, C. W.; Sieval, A. B.; Dakhorst, J. E. J.; van Dijk, M.; Kimkes, P.; Koehorst, R. B. M.; Donker, H.; Schaafsma, T. J.; Picken, S. J.; van de Craats, A. M.; Warman, J. M.; Zuilhof, H.; Sudhölter, E. J. R. Liquid Crystalline Perylene Diimides: Architecture and Charge Carrier Mobilities. *J. Am. Chem. Soc.* **2000**, *122*, 11057−11066.
(13) Singh, R.; Giussani, E.; Mróz, M. M.; Di Fonzo, F.; Fazzi, D.; Cabanillas-González, J.; Oldridge, L.; Vaenas, N.; Kontos, A. G.; Falaras, P.; Grimsdale, A. C.; Jacob, J.; Müllen, K.; Keivanidis, P. E. On the Role of Aggregation Effects in the Performance of Perylene-Diimide Based Solar Cells. *Org. Electron.* **2014**, *15*, 1347−1361.
(14) Tasios, N.; Grigoriadis, C.; Hansen, M. R.; Wonneberger, H.; Li, C.; Spiess, H. W.; Müllen, K.; Floudas, G. Self-Assembly, Dynamics, and Phase Transformation Kinetics of Donor−Acceptor Substituted Perylene Derivatives. *J. Am. Chem. Soc.* **2010**, *132*, 7478−7487.
(15) Chen, Z.; Baumeister, U.; Tschierske, C.; Würthner, F. Effect of Core Twisting on Self-Assembly and Optical Properties of Perylene Bisimide Dyes in Solution and Columnar Liquid Crystalline Phases. *Chem.—Eur. J.* **2007**, *13*, 450−465.
(16) Lindquist, R. J.; Lefler, K. M.; Brown, K. E.; Dyar, S. M.; Margulies, E. A.; Young, R. M.; Wasielewski, M. R. Energy Flow Dynamics within Cofacial and Slip-Stacked Perylene-3,4-dicarboximide Dimer Models of π-Aggregates. *J. Am. Chem. Soc.* **2014**, *136*, 14912−14923.
(17) Keivanidis, P. E.; Howard, I. A.; Friend, R. H. Intermolecular Interactions of Perylene Diimides in Photovoltaic Blends of Fluorene Copolymers: Disorder Effects on Photophysical Properties, Film Morphology and Device Efficiency. *Adv. Funct. Mater.* **2008**, *18*, 3189−3202.
(18) Brown, K. E.; Salamant, W. A.; Shoer, L. E.; Young, R. M.; Wasielewski, M. R. Direct Observation of Ultrafast Excimer Formation in Covalent Perylenediimide Dimers Using Near-Infrared Transient Absorption Spectroscopy. *J. Phys. Chem. Lett.* **2014**, *5*, 2588−2593.
(19) Vertsimakha, Y.; Lutsyk, P.; Palewska, K.; Sworakowski, J.; Lytvyn, O. Optical and Photovoltaic Properties of Thin Films of *N*,*N*′-Dimethyl-3,4,9,10-Perylenetetracarboxylic Acid Diimide. *Thin Solid Films* **2007**, *515*, 7950−7957.
(20) Pope, M.; Swenberg, C. E. *Electronic Processes in Organic Crystals and Polymers*. Oxford University Press: Oxford, UK, 1999.
(21) Ye, T.-L.; Singh, R.; Butt, H. J.; Floudas, G.; Keivanidis, P. E. Effect of Local and Global Structural Order on the Performance of Perylene Diimide Excimeric Solar Cells. *ACS Appl. Mater. Interfaces* **2013**, *5*, 11844−11857.
(22) Di Donato, E.; Fornari, R. P.; Di Motta, S.; Li, Y.; Wang, Z.; Negri, F. n-Type Charge Transport and Mobility of Fluorinated Perylene Bisimide Semiconductors. *J. Phys. Chem. B* **2010**, *114*, 5327−5334.
(23) Mizoshita, N.; Tani, T.; Inagaki, S. Highly Conductive Organosilica Hybrid Films Prepared from a Liquid-Crystal Perylene Bisimide Precursor. *Adv. Funct. Mater.* **2011**, *21*, 3291−3296.
(24) Takada, T.; Ashida, A.; Nakamura, M.; Fujitsuka, M.; Majima, T.; Yamana, K. Photocurrent Generation Enhanced by Charge Delocalization over Stacked Perylenediimide Chromophores Assembled within DNA. *J. Am. Chem. Soc.* **2014**, *136*, 6814−6817.
(25) Sharenko, A.; Proctor, C. M.; van der Poll, T. S.; Henson, Z. B.; Nguyen, T.-Q.; Bazan, G. C. A High-Performing Solution-Processed Small Molecule:Perylene Diimide Bulk Heterojunction Solar Cell. *Adv. Mater.* **2013**, *25*, 4403−4406.
(26) Sharenko, A.; Gehrig, D.; Laquai, F.; Nguyen, T.-Q. The Effect of Solvent Additive on the Charge Generation and Photovoltaic Performance of a Solution-Processed Small Molecule:Perylene Diimide Bulk Heterojunction Solar Cell. *Chem. Mater.* **2014**, *26*, 4109−4118.
(27) Singh, R.; Aluicio-Sarduy, E.; Kan, Z.; Ye, T.; MacKenzie, R. C. I.; Keivanidis, P. E. Fullerene-Free Organic Solar Cells with an Efficiency of 3.7% Based on a Low-Cost Geometrically Planar Perylene Diimide Monomer. *J. Mater. Chem. A* **2014**, *2*, 14348−14353.
(28) Sun, Y.; Seo, J. H.; Takacs, C. J.; Seifter, J.; Heeger, A. J. Inverted Polymer Solar Cells Integrated with a Low-Temperature-Annealed Sol−Gel-Derived ZnO Film as an Electron Transport Layer. *Adv. Mater.* **2011**, *23*, 1679−1683.
(29) Lu, Z.; Jiang, B.; Zhang, X.; Tang, A.; Chen, L.; Zhan, C.; Yao, J. Perylene−Diimide Based Non-Fullerene Solar Cells with 4.34% Efficiency through Engineering Surface Donor/Acceptor Compositions. *Chem. Mater.* **2014**, *26*, 2907−2914.
(30) Zang, Y.; Li, C.-Z.; Chueh, C.-C.; Williams, S. T.; Jiang, W.; Wang, Z.-H.; Yu, J.-S.; Jen, A. K. Y. Integrated Molecular, Interfacial, and Device Engineering towards High-Performance Non-Fullerene Based Organic Solar Cells. *Adv. Mater.* **2014**, *26*, 5708−5714.
(31) Singh, R.; Mróz, M. M.; Di Fonzo, F.; Cabanillas-Gonzalez, J.; Marchi, E.; Bergamini, G.; Müllen, K.; Jacob, J.; Keivanidis, P. E. Improving the Layer Morphology of Solution-Processed Perylene Diimide Organic Solar Cells with the Use of a Polymeric Interlayer. *Org. Photonics Photovoltaics* **2013**, *1*, 24−38.
(32) Zhao, J.; Li, Y.; Lin, H.; Liu, Y.; Jiang, K.; Mu, C.; Ma, T.; Lai, J. Y. L.; Yan, H. High-Efficiency Non-Fullerene Organic Solar Cells Enabled by a Difluorobenzothiadizole-Based Donor Polymer Combined with a Properly Matched Small Molecule Acceptor. *Energy Environ. Sci.* **2015**, *8*, 520−525.
(33) Wakim, S.; Beaupre, S.; Blouin, N.; Aich, B.-R.; Rodman, S.; Gaudiana, R.; Tao, Y.; Leclerc, M. Highly Efficient Organic Solar Cells based on a Poly(2,7-carbazole) Derivative. *J. Mater. Chem.* **2009**, *19*, 5351−5358.
(34) Berti, G.; Calloni, A.; Brambilla, A.; Bussetti, G.; Duò, L.; Ciccacci, F. Direct Observation of Spin-Resolved Full and Empty Electron States in Ferromagnetic Surfaces. *Rev. Sci. Instrum.* **2014**, *85*, 073901.
(35) Xu, Z.; Chen, L.-M.; Yang, G.; Huang, C.-H.; Hou, J.; Wu, Y.; Li, G.; Hsu, C.-S.; Yang, Y. Vertical Phase Separation in Poly(3-hexylthiophene): Fullerene Derivative Blends and Its Advantage for Inverted Structure Solar Cells. *Adv. Funct. Mater.* **2009**, *19*, 1227−1234.
(36) Jones, C. M.; Donnelly, P. E.; Schwartz, J. A Nanoscale Interface Improves Attachment of Cast Polymers to Glass. *ACS Appl. Mater. Interfaces* **2010**, *2*, 2185−2188.
(37) Brambilla, A.; Calloni, A.; Aluicio-Sarduy, E.; Berti, G.; Kan, Z.; Beaupré, S.; Leclerc, M.; Butt, H. J.; Floudas, G.; Keivanidis, P. E.; Duò, L. X-ray Photoemission Spectroscopy Study of Vertical Phase Separation in F8BT:PDI/ITO Films for Photovoltaic Applications. *Proc. SPIE* **2014**, 91650C DOI: 10.1117/12.2063929.

DOI: 10.1021/acsami.5b00827
ACS Appl. Mater. Interfaces 2015, 7, 8687−8698

(38) Guo, X.; Puniredd, S. R.; He, B.; Marszalek, T.; Baumgarten, M.; Pisula, W.; Müllen, K. Combination of Two Diketopyrrolopyrrole Isomers in One Polymer for Ambipolar Transport. *Chem. Mater.* **2014**, *26*, 3595−3598.
(39) Sun, K.; Xiao, Z.; Lu, S.; Zajaczkowski, W.; Pisula, W.; Hanssen, E.; White, J. M.; Williamson, R. M.; Subbiah, J.; Ouyang, J.; Holmes, A. B.; Wong, W. W. H.; Jones, D. J. A Molecular Nematic Liquid Crystalline Material for High-Performance Organic Photovoltaics. *Nat. Commun.* **2015**, *6*, 6013−6021.
(40) Chen, C.-S.; Yang, P.-C.; Shen, Y.-M.; Ma, S.-Y.; Shiou, S.-C.; Hung, S.-C.; Lin, S.-H.; Lin, C.-F. The Influence of Wrinkled ZnO on Inverted Low Bandgap Thin Film Solar Cells. *Sol. Energy Mater. Sol. Cells* **2012**, *101*, 180−185.
(41) Keivanidis, P. E.; Kamm, V.; Dyer-Smith, C.; Zhang, W.; Laquai, F.; McCulloch, I.; Bradley, D. D. C.; Nelson, J. Delayed Luminescence Spectroscopy of Organic Photovoltaic Binary Blend Films: Probing the Emissive Non-Geminate Charge Recombination. *Adv. Mater.* **2010**, *22*, 5183−5187.
(42) Hayer, A.; de Halleux, V.; Köhler, A.; El-Garoughy, A.; Meijer, E. W.; Barberá, J.; Tant, J.; Levin, J.; Lehmann, M.; Gierschner, J.; Cornil, J.; Geerts, Y. H. Highly Fluorescent Crystalline and Liquid Crystalline Columnar Phases of Pyrene-Based Structures. *J. Phys. Chem. B* **2006**, *110*, 7653−7659.
(43) Gierschner, J.; Mack, H.-G.; Oelkrug, D.; Waldner, I.; Rau, H. Modeling of the Optical Properties of Cofacial Chromophore Pairs: Stilbenophane. *J. Phys. Chem. A* **2004**, *108*, 257−263.
(44) Dittmer, J. J.; Marseglia, E. A.; Friend, R. H. Electron Trapping in Dye/Polymer Blend Photovoltaic Cells. *Adv. Mater.* **2000**, *12*, 1270−1274.
(45) Martinelli, N. G.; Olivier, Y.; Athanasopoulos, S.; Ruiz Delgado, M.-C.; Pigg, K. R.; da Silva Filho, D. A.; Sánchez-Carrera, R. S.; Venuti, E.; Della Valle, R. G.; Brédas, J.-L.; Beljonne, D.; Cornil, J. Influence of Intermolecular Vibrations on the Electronic Coupling in Organic Semiconductors: The Case of Anthracene and Perfluoropentacene. *ChemPhysChem* **2009**, *10*, 2265−2273.
(46) Baranovskii, S. D. Theoretical Description of Charge Transport in Disordered Organic Semiconductors. *Phys. Status Solidi B* **2014**, *251*, 487−525.
(47) Gehrig, D.; Roland, S.; Howard, I. A.; Kamm, V.; Mangold, H.; Neher, D.; Laquai, F. Efficiency-Limiting Processes in Low-Bandgap Polymer:Perylene Diimide Photovoltaic Blends. *J. Phys. Chem. C* **2014**, *118*, 20077−20085.
(48) Koster, L. J. A.; Mihailetchi, V. D.; Ramaker, R.; Blom, P. W. M. Light Intensity Dependence of Open-Circuit Voltage of Polymer:-Fullerene Solar Cells. *Appl. Phys. Lett.* **2005**, *86*, 123509/1−123509/3.
(49) Kirchartz, T.; Pieters, B. E.; Kirkpatrick, J.; Rau, U.; Nelson, J. Recombination via Tail States in Polythiophene:Fullerene Solar Cells. *Phys. Rev. B* **2011**, *83*, 115209.
(50) Blakesley, J. C.; Neher, D. Relationship Between Energetic Disorder and Open-Circuit Voltage in Bulk Heterojunction Organic Solar Cells. *Phys. Rev. B* **2011**, *84*, 075210.

DOI: 10.1021/acsami.5b00827
ACS Appl. Mater. Interfaces 2015, 7, 8687−8698